



Research article

Non-thermal plasma-treated melatonin inhibits the biological activity of HCC cells by increasing intracellular ROS levels and reducing RRM2 expression

Bangjie Chen^{a,1}, Tao Jin^{b,1}, Ziyue Fu^{c,1}, Haiwen Li^{d,1}, Junfa Yang^e, Yucheng Liu^a, Yanxun Han^a, Xinyi Wang^a, Zhengwei Wu^{b,f,*}, Tao Xu^{g,h,**}

^a First Affiliated Hospital of Anhui Medical University, Hefei, China

^b School of Nuclear Science and Technology, University of Science and Technology of China, Hefei, China

^c Second Clinical School of Anhui Medical University, Hefei, China

^d Third Affiliated Hospital of Anhui Medical University, Hefei, China

^e Second Affiliated Hospital of Zhejiang University, Hangzhou, Zhejiang, China

^f CAS Key Laboratory of Geospace Environment, University of Science and Technology of China, Hefei, China

^g Inflammation and Immune Mediated Diseases Laboratory of Anhui Province; School of Pharmacy, Anhui Medical University, Hefei, China

^h Institute for Liver Diseases of Anhui Medical University, Hefei, China



ARTICLE INFO

Keywords:

Non-thermal plasma

Melatonin

Ribonucleotide reductase regulatory subunit

M2

Reactive oxygen species

Oncotherapy

ABSTRACT

Non-thermal plasma (NTP) is thought to have a cytotoxic effect on tumor cells. Although its application in cancer therapy has shown considerable promise, the current understanding of its mechanism of action and cellular responses remains incomplete. Furthermore, the use of melatonin (MEL) as an adjuvant anticancer drug remains unexplored. In this study, we found that NTP assists MEL in promoting apoptosis, delaying cell cycle progression, and inhibiting cell invasion and migration in hepatocellular carcinoma (HCC) cells. This mechanism may be associated with the regulation of intracellular reactive oxygen species levels and ribonucleotide reductase regulatory subunit M2 expression. Our findings confirm the pharmacological role of MEL and the adjuvant value of NTP, emphasizing their potential in combination therapy for HCC. Our study may have important implications for the development of new approaches for HCC treatment.

1. Introduction

Non-thermal plasma (NTP) is an ionized gas composed of charged particles, electronically excited atoms, molecules, free radicals, and ultraviolet photons [1]. NTP is believed to generate reactive oxygen species (ROS) that trigger DNA damage and mitochondrial dysfunction and inhibit tumor cell metabolism, thereby inducing tumor cell death [2,3]. Several studies have shown that NTP exhibits antitumor activity against various cancers, such as colorectal cancer, leukemia, and mesothelioma [4–6]. NTP in combination with drugs or chemotherapy has attracted increasing attention as a potential tumor treatment method.

* Corresponding author. School of Nuclear Science and Technology, University of Science and Technology of China, Hefei, China,

** Corresponding author. Inflammation and Immune Mediated Diseases Laboratory of Anhui Province; School of Pharmacy, Anhui Medical University, Hefei, China,

E-mail addresses: wuzw@ustc.edu.cn (Z. Wu), xutao@ahmu.edu.cn (T. Xu).

¹ These authors contributed equally.

<https://doi.org/10.1016/j.heliyon.2023.e15992>

Received 10 December 2022; Received in revised form 27 April 2023; Accepted 28 April 2023

Available online 3 May 2023

2405-8440/© 2023 Published by Elsevier Ltd.

This is an open access article under the CC BY-NC-ND license

(<http://creativecommons.org/licenses/by-nc-nd/4.0/>).

Hepatocellular carcinoma (HCC) is the leading cause of death in patients with liver cirrhosis and the fourth leading cause of cancer deaths worldwide [7]. Despite current advances in HCC treatment, there remains a lack of effective treatments for improving the survival of patients with intermediate and advanced HCC [7]. Current radical treatments for HCC include surgical resection, liver transplantation, and locoregional therapies such as ablation and embolization. Although these treatments have shown some efficacy in

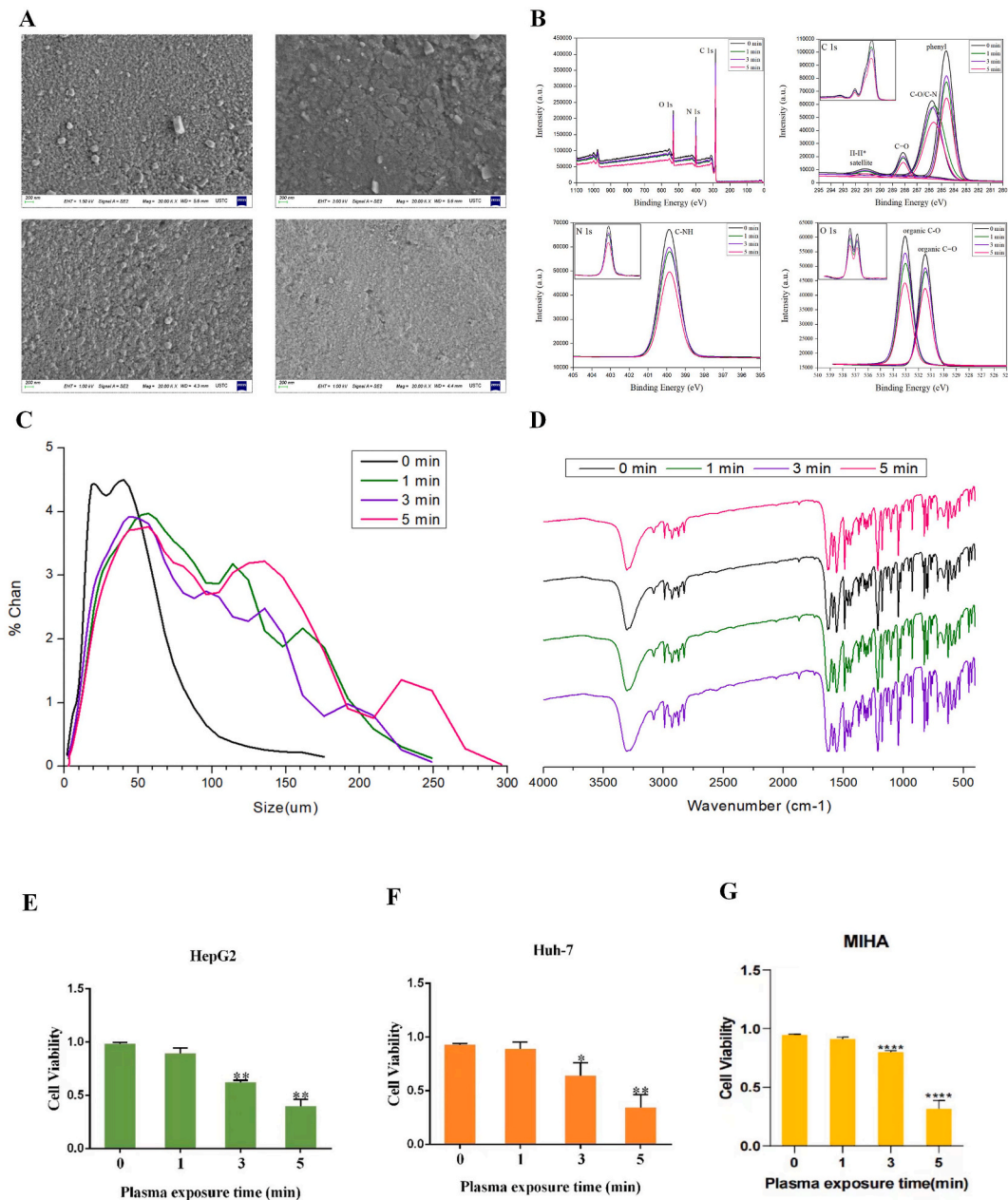


Fig. 1. (A) Scanning electron microscopy (SEM) analysis showed that with the increase of NTP treatment time, the surface of MEL slices was smoother and particle size gradually increased; (B) X-ray photoelectron spectroscopy (XPS) analysis showed three strong waves at around 285 eV, 400 eV and 530 eV, which were mainly the binding energies of C1s, N1s and O1s. Three binding energy standard peaks (phenyl group 1, C–O/C–N, C=O) of C1s at 284.5, 286, and 288 eV, one binding energy standard peak (C–NH) of N1s at 400 eV, and two binding energy standard peaks (C–O, C=O) of O1s at 531 eV and 533 eV all decreased with increasing treatment time. But when NTP treatment was used for 1 min, but still lower than that when NTP was not used to treat; (C) laser particle size analysis showed that from the NTP-0min group (0–180 μm) to NTP-5min group (0–300 μm), the MEL particle size range was gradually expanded; (D) the IR spectra of the NTP-0min, NTP-1min, NTP-3min, and NTP-5min groups (Fig. 1D), with a clear peak at 3250 cm⁻¹; (E–G) CCK8 assay results showed that melatonin treated with NTP for 3 and 5 min inhibited the viability of HepG2, Huh-7 and MIHA cells more significantly than melatonin without NTP treatment (*p < 0.05, **p < 0.01).

early stage HCC, their efficacy is often limited by factors such as tumor size, tumor location, and underlying liver dysfunction. Radiotherapy is another treatment option for HCC, particularly for patients who are not surgical candidates. However, radiotherapy is limited by its potential toxicity to the surrounding healthy tissues, which can cause liver dysfunction, thus limiting the total dose that can be delivered. Immunotherapy and targeted therapy have also shown promise for the treatment of advanced HCC; however, only a subset of patients respond to these treatments, and the development of resistance is a common challenge. Moreover, the use of immunotherapy in patients with hepatitis B or C viral infections requires careful consideration owing to the risk of viral reactivation [8]. Therefore, it is essential to explore and develop new therapeutic approaches for HCC to overcome these limitations and improve patient outcomes. Ribonucleotide reductase regulatory subunit M2 (RRM2) catalyzes deoxyribonucleotide production during DNA synthesis and is a potential prognostic marker in glioma, breast cancer, and prostate cancer [9–11]. Zhou et al. screened HCC-related prognostic markers and found that RRM2 was significantly enriched in the p53 signaling pathway, an important tumor suppressor gene pathway [12]. However, the specific mechanism of action of RRM2 in HCC remains unclear and requires further exploration.

Melatonin (MEL) is an indoleamine with multiple biological functions that is secreted primarily by the pineal gland in humans and other mammals to adapt to darkness [13]. Other organs that synthesize MEL include the retina, gastrointestinal tract, skin, bone marrow and lymphocytes [14]. MEL levels increase at night and decrease during the day. The suprachiasmatic nucleus of the hypothalamus regulates MEL synthesis and secretion to regulate metabolism and defend against various diseases [15]. In addition to being a hormone, MEL is also thought to play a role in oxidative stress, immune regulation, and hematopoiesis [16,17]. MEL exerts anticancer effects by inducing cell apoptosis, inhibiting proliferation, tumor invasion, and metastasis, reducing the side effects of radiotherapy and tumor resistance, and enhancing therapeutic effects [18–20]. Furthermore, MEL can be used in combination with conventional treatments to enhance their efficacy and reduce side effects and has great potential as an adjuvant treatment for cancer [21].

The objective of this study was to investigate the efficacy and mechanism of synergistic NTP and MEL treatment for HCC. Our study showed that NTP-treated MEL is more effective against HCC, thus confirming the value of drug combinations. Additionally, we found that the mechanism underlying the synergistic anticancer effect of NTP and MEL may involve regulation of intracellular ROS and RRM2 expression levels. Overall, our study provides new avenues and ideas for future tumor therapies.

2. Method

2.1. Cell culture and reagents

Two human HCC cell lines (HepG2 and Huh-7) and human normal liver cell line (MIHA) were purchased from ATCC (Manassas, VA, USA) and were cultured in Dulbecco's modified eagle's medium containing 10% fetal bovine serum (Gibco, Waltham, MA, USA) and 100 U ml⁻¹ penicillin-streptomycin (Gibco). The culture environment was maintained at 5% CO₂ and 37 °C in humidified air. The culture medium was changed three times per week.

MEL was purchased from Sigma-Aldrich (Darmstadt, Germany). Primary antibodies for RRM2, β -actin, Bax, Bcl-2, proliferating cell nuclear antigen (PCNA), matrix metalloproteinase-2 (MMP2), matrix metalloproteinase-9 (MMP9), Caspase 3 and p53 were purchased from Cell Signaling Technology (Beverly, MA, USA).

2.2. Patient and tissue collection

The Biomedical Ethics Committee of Anhui Medical University approved this study (20,210,683). Liver tissues were obtained from the General Surgery Department of The First Affiliated Hospital of Anhui Medical University. All patients were diagnosed with HCC according to WHO standards [22] and received radical surgery [23]. The surgical specimens were immediately placed in liquid nitrogen for quick freezing and then stored in a -80 °C refrigerator. Written informed consent was obtained from all participants.

2.3. Treatment using non-thermal dielectric barrier discharge plasma

As shown in Fig. 1A and mg of MEL powder (Sigma-Aldrich) was used to prepare slices that were subsequently exposed to He plasma for 1, 3, or 5 min, and labelled as P1, P3, and P5, respectively. Untreated MEL was used as a control. The gas flow rate of the injected He was set to 2 L/min, and the working current, voltage, and frequency of the He-plasma device were 0.488 A, 12.4 kV, and 1.0 kHz, respectively (Figure S1). Following He-plasma exposure, the MEL slices were ground into a powder again in 10 min and immediately used to prepare the MEL solution for later HCC experiments.

2.4. Material characterization analysis

Scanning electron microscopy analysis was performed at various magnifications. Images of the MEL sections were recorded using a scanning electron microscope (GeminiSEM 500, Oberkochen, Germany). A Microtrac S3500 synchronous laser diffraction and dynamic image particle analyzer (Microtrac, Montgomeryville, PA, USA) was used to analyze the change in particle size in MEL slices treated with NTP for different times, and the measured particle size ranged from 0.01 to 2800 μ m. The relative contents of various functional groups in MEL treated with NTP for different durations were determined using a Thermo ESCALAB250Xi spectrometer (Thermo Fisher Scientific, Waltham, MA, USA). A Fourier transform infrared spectrometer (Thermo Fisher Scientific) was used in the wavelength range of 4000–400 cm⁻¹ to determine changes in the functional groups of MEL after NTP treatment for different times.

2.5. Cell viability assay

Cells were inoculated into culture dishes at a density of 3×10^5 and placed in medium overnight before MEL was used. MEL treated with NTP for different times (0, 1, 3, and 5 min) was added to HepG2 and Huh-7 cells. After 24 h, the CCK-8 kit was used to determine cell viability, and a Varioskan Flash microplate reader (Thermo Fisher Scientific) was used to measure the absorbance at 450 nm. Cell viability was calculated using the following formula: % cell growth = [(OD492 of control-OD492 of sample)/OD492 of control]*100 [24,25].

2.6. Transcriptome sequencing

Total RNA was extracted from the samples using Trizol reagent (Invitrogen, Waltham, MA, USA), and the RNA quality was assessed using a NanoDrop spectrophotometer (Thermo Scientific) and an Agilent 2100 Bioanalyzer (Agilent Technologies, Santa Clara, CA, USA). Poly(A) mRNA was enriched using oligo (dT) beads, and cDNA libraries were prepared using the TruSeq Stranded mRNA Library Prep Kit (Illumina, San Diego, CA, USA) according to the manufacturer's protocol. The cDNA libraries were sequenced on the Illumina HiSeq X Ten platform with paired-end reads of 150 bp. Quality control of the raw data was performed using FastQC, and the reads were trimmed and filtered using Trimmomatic. The clean reads were aligned to the reference genome using HISAT2, and gene expression levels were quantified using StringTie. Differential expression analysis was performed using the DESeq2 package. Kyoto Encyclopedia of Genes and Genomes (KEGG) pathway analysis was performed using the clusterProfiler package.

2.7. siRNA transfection

The siRNA target sequence of RRM2 is: forward (F) primer sequence 5'-GTGGAGCGATTTAGCCAAGAA-3' and reverse (R) primer sequence 5'-CACAAAGCA-TCGTTTCAATGG-3'. Human Huh-7 cells seeded in 35-mm dishes (50–60% confluency) were transfected with Lipofectamine 2000 (Invitrogen) according to the manufacturer's instructions, and the transfection mixture was added to the culture medium for cell culture. The cells were collected after 48 h of incubation.

2.8. Flow cytometry assay

Human Huh-7 cells were collected by trypsinization, washed twice in cold phosphate-buffered saline (PBS), suspended in 1 Annexin V binding buffer (500 L), and stained using Annexin V-FITC and PI from the Apoptosis Detection Kit I (BD Biosciences, San Jose, CA, USA). A flow cytometer (BD Biosciences) was used to identify apoptosis, and FACS Suite software was used to analyze the results. The cells were trypsinized and fixed in 75% ice-cold ethanol in PBS for cell cycle testing. Bovine pancreatic RNase (2 mg/ml; Sigma-Aldrich) and propidium iodide (10 mg/ml; Invitrogen) were added to the cells. The cells were then kept in the dark and incubated at room temperature (20–25 °C) for 30 min. The flow cytometer (BD Biosciences) was used to examine cell dispersion. For the detection of intracellular ROS, cells were harvested by trypsinization and cultured with serum-free medium containing DCFH-DA for 20 min at 37 °C. After centrifugation at 300g for 5 min, the supernatant was discarded, and the cells were washed three times with PBS. The intensity of the DCF signal was detected by flow cytometry (BD Biosciences) to quantify intracellular ROS generation.

2.9. Wound healing assay

Human Huh-7 cells in the logarithmic growth phase were inoculated with 1×10^6 /ml cell count in six-well plates at passaging 3–5, and placed in an incubator for 24 h. Cells were collected when the growth reached 70%. A minor horizontal scratch was made on the bottom surface of adherent cells using a 10- μ l autoclaved pipette tip. The cells were gently washed twice with PBS to remove detached cells. The plates were incubated in an incubator for 24 h. The cells were fixed with a methanol solution and stained with crystalline violet. An inverted microscope was used to observe the healing of the cell scratch during photography and recording.

2.10. Transwell assay

Human Huh-7 cells were introduced into the top chamber using a serum-free medium, and each well contained 2×10^6 cells. Additionally, 500 μ L 20% fetal bovine serum medium was added to the bottom chamber. After incubation with 5% (v/v) CO₂ at 37 °C for 2 days, non-invasive cells and matrix glue were removed from the top chamber. The cells were fixed to the bottom surface with 10% neutral-buffered formalin solution and stained with 0.1% crystal violet. The number of invading cells was calculated in five randomly selected microscopic fields.

2.11. Western blotting

The cells were lysed using RIPA lysis buffer after rinsing with cold PBS (Beyotime, Shanghai, China). The supernatant was collected after the lysates were centrifuged at 12,000 rpm for 10 min at 4 °C. The BCA Protein Assay Reagent Kit was used to measure the protein concentration (Beyotime). Equal amounts of protein were extracted using 8–12% SDS-PAGE and applied to a polyvinylidene difluoride membrane (Millipore Corporation, Burlington, MA, USA). The membranes were then incubated with specific primary antibodies overnight at 4 °C, blocked with 5% nonfat milk powder, and tagged with IRDye-conjugated secondary antibodies for 1 h at room

temperature (20–25 °C). Odyssey CLx (LI-COR, Lincoln, NE, USA) was used to measure the membranes.

2.12. JC-1 staining

Human Huh-7 cells were seeded at a density of 1×10^4 cells/well in 96-well plates and allowed to adhere overnight. The cells were then treated with the desired treatment for 24 h. The cells were washed twice with phosphate-buffered saline (PBS) and then incubated with 10 µg/ml JC-1 dye (Beyotime) in culture medium at 37 °C for 30 min. The cells were then washed twice with PBS and analyzed using a fluorescence microscope (Nikon, Tokyo, Japan) with excitation and emission wavelengths of 488 nm and 525 nm for the monomeric form (green), and 525 nm and 590 nm for the aggregated form (red).

2.13. TUNEL staining

The terminal deoxynucleotidyl transferase-mediated dUTP nick-end labeling (TUNEL) assay was performed to detect apoptotic cells. Human Huh-7 cells were seeded in 24-well plates at a density of 1×10^5 cells/well and allowed to adhere overnight. The cells were then treated with the desired treatment for 24 h. The cells were fixed with 4% paraformaldehyde for 30 min at room temperature (20–25 °C) and permeabilized with 0.1% Triton X-100 in PBS for 5 min. The TUNEL assay was performed using the In Situ Cell Death Detection Kit (Roche, Basel, Switzerland) according to the manufacturer's instructions. The images were captured using a fluorescence microscope (Nikon) with excitation and emission wavelengths of 488 nm and 525 nm for green fluorescence. The TUNEL-positive cells were quantified by counting the number of green fluorescent cells per high-power field (HPF).

2.14. Caspase 3 immunofluorescence staining

Human Huh-7 cells were seeded in 24-well plates at a density of 1×10^5 cells/well and allowed to adhere overnight. The cells were then treated with the desired treatment for 24 h. The cells were fixed in 4% paraformaldehyde and permeabilized in 0.1% Triton X-100 in PBS to allow the immunostaining reagents to penetrate into the cells. The cells were then incubated with a primary antibody against Caspase 3 (diluted 1:500) overnight at 4 °C, followed by incubation with a fluorescent secondary antibody (diluted 1:1000, Alexa Fluor 488 goat anti-rabbit IgG, Invitrogen) for 1 h at room temperature (20–25 °C). The cells were then washed three times and counterstained with DAPI (4',6-diamidino-2-phenylindole) nuclear stain. Fluorescence images were acquired using a fluorescence microscope (Nikon).

2.15. Statistical analysis

Data are presented as mean standard deviation (SD), and all experiments were repeated at least three times. Differences between the outcomes of the two groups were assessed using the Student's t-test, and $P < 0.05$ was regarded as statistically significant.

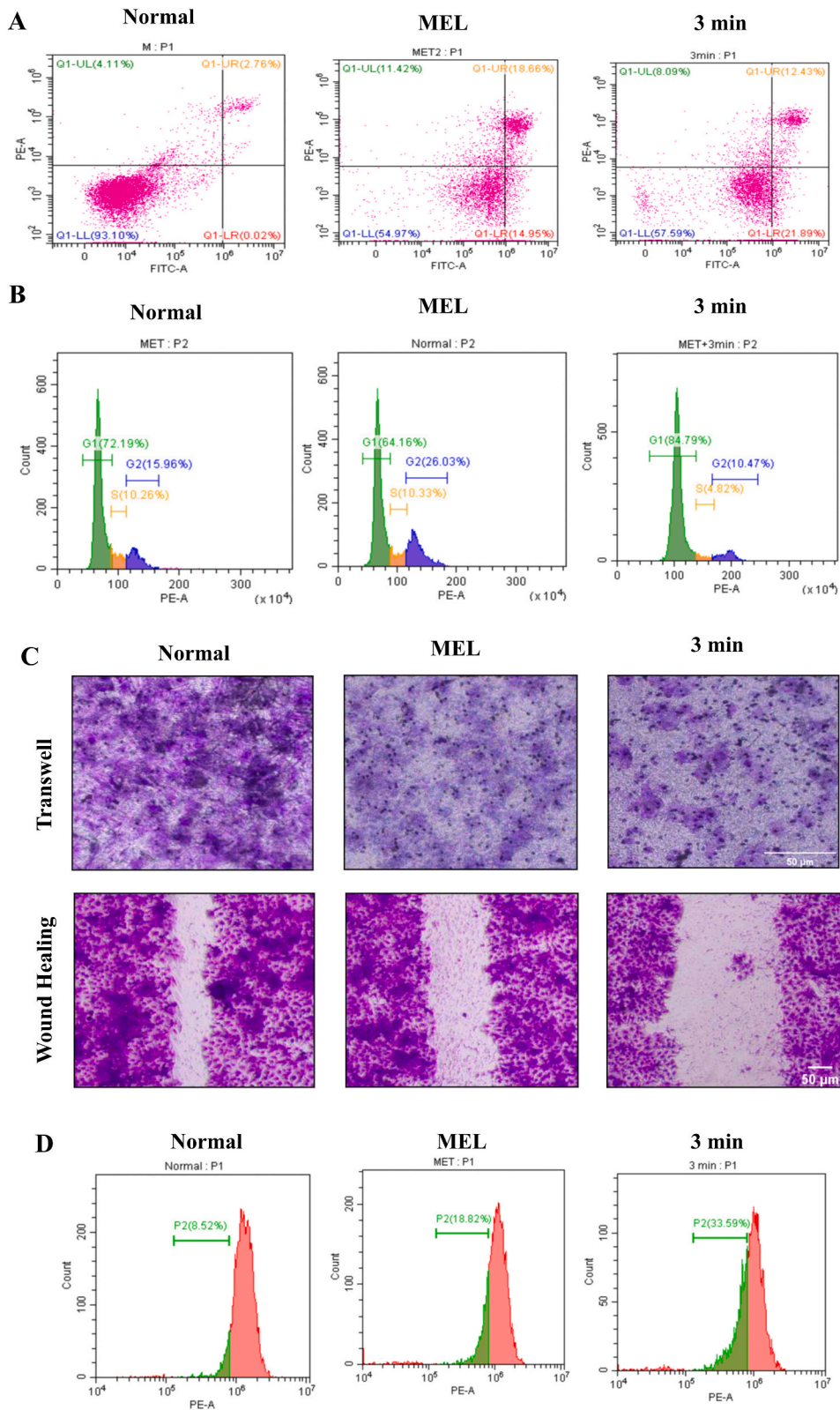
3. Results

3.1. Material characterization of NTP-treated MEL

As shown in Fig. 1A, as NTP treatment time increased, the surface of the MEL slices became smoother and the particle size gradually increased, which may have been caused by the enhanced electrostatic adsorption of the particles due to the change in chemical groups during the NTP treatment. This is consistent with the results of laser particle size analysis (Fig. 1C). The MEL particle size range gradually increased from the NTP-0 min group (0–180 µm) to the NTP-5 min group (0–300 µm). X-ray photoelectron spectroscopy (XPS) analysis (Fig. 1B) revealed three stronger waves near 285, 400, and 530 eV, which were mainly the binding energies of C1s, N1s, and O1s. Fig. 1B shows that the three standard peaks of C1s as phenyl, C–O/C–N, and C=O binding energies at 284.5, 286, and 288 eV, respectively, decreased with increasing treatment time. Additionally, N1s as C–NH and O1s as C–O and C=O binding energies had significant peaks around 400, 531, and 533 eV, respectively, and the intensity showed a downward trend with increasing exposure time. However, when NTP was used for treatment for 3 min, the intensity of all peaks increased, which was higher than that when NTP was used for treatment for 1 min, but still lower than that when NTP was not used for treatment. We also obtained the IR spectra of the NTP-0 min, NTP-1 min, NTP-3 min, and NTP-5 min groups (Fig. 1D), with a clear peak at 3250 cm^{-1} .

3.2. NTP assists MEL in suppressing HCC and MIHA cell viability

We stimulated HCC (HepG2 and Huh-7) and MIHA cells with MEL without NTP treatment and with MEL treated with NTP for different durations (1, 3, or 5 min) for 24 h. The results of the CCK8 assay showed that there was no difference between MEL treated with NTP for 1 min and MEL without NTP treatment in terms of its effect on the viability of HCC cells. However, MEL treatment with NTP for 3 and 5 min inhibited the viability of HepG2, Huh-7 and MIHA cells more significantly than MEL treatment without NTP (Fig. 1E–G). Therefore, in subsequent experiments, we selected 3 min as the optimal time for NTP treatment of MEL.



(caption on next page)

Fig. 2. (A) Flow cytometry results showed that compared with the control group, the apoptotic rate of Huh-7 cells was significantly increased with MEL treatment; while the apoptotic rate of Huh-7 cells was further increased with the NTP-treated MEL treatment; (B) Flow cytometry results showed that the G1 phase of Huh-7 cells treated with MEL was significantly increased and the S phase was decreased; while NTP-treated MEL further increased the G1 phase and further decreased the S phase; (C) Transwell and wound healing assays showed that MEL can inhibit the invasion and migration of Huh-7 cells, and NTP-treated MEL will further enhance the inhibition effect (The scratch area was 30033.186, 29802.735, 52293.397 μm^2 in turn from left to right); (D) Flow cytometry (DCFH-DA fluorescence staining method) detection showed that MEL could increase the level of intracellular ROS in Huh-7 cells, and the ability of NTP-treated MEL to increase intracellular ROS was further enhanced.

3.3. NTP assists MEL in promoting HCC cell apoptosis, delaying cell cycle progression, and inhibiting cell invasion and migration

As shown in Fig. 2A, compared to the control group, the apoptotic rate of Huh-7 cells was significantly increased by MEL treatment and was increased to an even greater extent with NTP-treated MEL treatment. In terms of cell cycle progression, the G1 phase of Huh-7 cells treated with MEL significantly increased and the S phase decreased, whereas NTP-treated MEL further increased the G1 phase and decreased the S phase (Fig. 2B). The results of both the transwell and wound healing assays separately showed that MEL inhibited the invasion and migration of Huh-7 cells, and NTP-treated MEL further enhanced the inhibitory effect (Fig. 2C).

3.4. NTP assists MEL in increasing intracellular ROS levels

As shown in Fig. 2D, flow cytometry (DCFH-DA fluorescence staining) showed that MEL increased intracellular ROS levels in Huh-7 cells, and the ability of NTP-treated MEL to increase intracellular ROS was further enhanced. Increased ROS levels in HCC cells promote apoptosis.

3.5. NTP and MEL synergistically regulate RRM2 expression

As shown in the results of transcriptome sequencing in Fig. 3A, H7_3min was the control group, and H7_MEL was the experimental group, the volcano plot results showed nine upregulated and nine downregulated genes. The results of heat map analysis also showed differences in cellular gene expression under the influence of MEL and NTP-treated MEL (Fig. 3B). Western blotting was performed using HCC and adjacent normal liver tissues, MIHA cells, and Huh-7 cells. The RRM2 gene was upregulated in HCC tissues and Huh-7 cells, suggesting that RRM2 is involved in tumor progression (Fig. 3C and D). We performed RRM2 siRNA transfection on Huh-7 cells. Compared to the RRM2 negative control (NC), flow cytometry revealed a significantly higher rate of apoptosis in Huh-7 cells in the RRM2 siRNA group (Fig. 3E), which was also confirmed by Western blot analysis of Bcl-2 and Bax (Fig. 4B). In addition, the same results were also obtained from JC-1 staining (Figure S1A), Caspase 3 immunofluorescence staining (Figure S1B), and TUNEL staining (Figure S1C). EdU staining revealed that RRM2 siRNA inhibited the proliferation of Huh-7 cells (Fig. 3F), which was also confirmed by Western blot analysis of PCNA (Fig. 4C). Finally, we performed Transwell and wound healing assays. The results showed that RRM2 siRNA significantly inhibited Huh-7 cell invasion and migration (Fig. 4A), consistent with the expression of MMP2 and MMP9 (Fig. 4C). KEGG pathway enrichment analysis based on transcriptome sequencing was performed on RRM2, and it was found that p53 might be a downstream signaling pathway of RRM2 (Fig. 4D), which was also confirmed by western blotting (Fig. 4E).

4. Discussion

The relationship between MEL and cancer has been explored for a long time [26]. MEL has been shown to slow cancer progression, and several potential mechanisms have been suggested [27]. MEL binds to two types of receptors belonging to the G-protein superfamily that mediate its anticancer effects by inhibiting linoleic acid uptake [28]. The receptor-independent mechanism by which MEL exerts anticancer effects involves immunomodulation, anti-angiogenesis, modulation of MT1 and MT2 membrane receptor signaling processes, reduction in growth factor uptake, promotion of oxidative metabolism, and antioxidant activity [29,30]. It has also been suggested that MEL increases the sensitivity of cancer cells to radiotherapy, thereby increasing its therapeutic effect [31]. MEL shows considerable potential as an adjuvant treatment for cancer in clinical practice, especially for the treatment of HCC. MEL inhibits linoleic acid uptake by activating MT1 and MT2 receptors and preventing the formation of 1,3-hydroxyoctadecenoic acid, a mitotic metabolite, thus inhibiting the progression of HCC cells [28]. Moreover, current liver cancer treatment is hindered by drug resistance and distant metastasis in advanced stages of cancer, and MEL is an effective adjuvant therapy to address both problems. MEL effectively limits the invasion of cancer cells into the vasculature and prevents distant metastasis [32]. To confirm whether MEL has an antitumor adjuvant effect, we used NTP-treated MEL cells to verify its efficacy against HCC. Our findings support this view, and provide ideas and bases for the design of new therapies to treat and prevent cancer using MEL in the future (Fig. 5).

NTP has numerous medical applications in hemostasis, angiogenesis, organ adhesion and cell proliferation [33]. NTP is currently considered a potential tumor therapy; however, its mechanism of action remains unclear. The antitumor effect of NTP appears to be largely attributable to oxidative stress. This hypothesis suggests that NTP can induce oxidative stress in cells and tissues by generating ROS and reactive nitrogen species and that ROS play an important role in inducing apoptosis [34]. ROS are known to affect multiple cellular signaling pathways, including cell proliferation, differentiation, and apoptosis [35]. ROS are usually produced at higher levels in tumor cells than in normal cells [36]. Although higher ROS levels can promote tumor progression to a certain extent, it also makes tumor cells more susceptible to NTPs than normal cells [37]. High levels of ROS and oxidative stress lead to DNA double-strand breaks and the inhibition of metabolic activity, leading to apoptosis [38]. Barborá et al. explored the detailed mechanisms of NTP-mediated

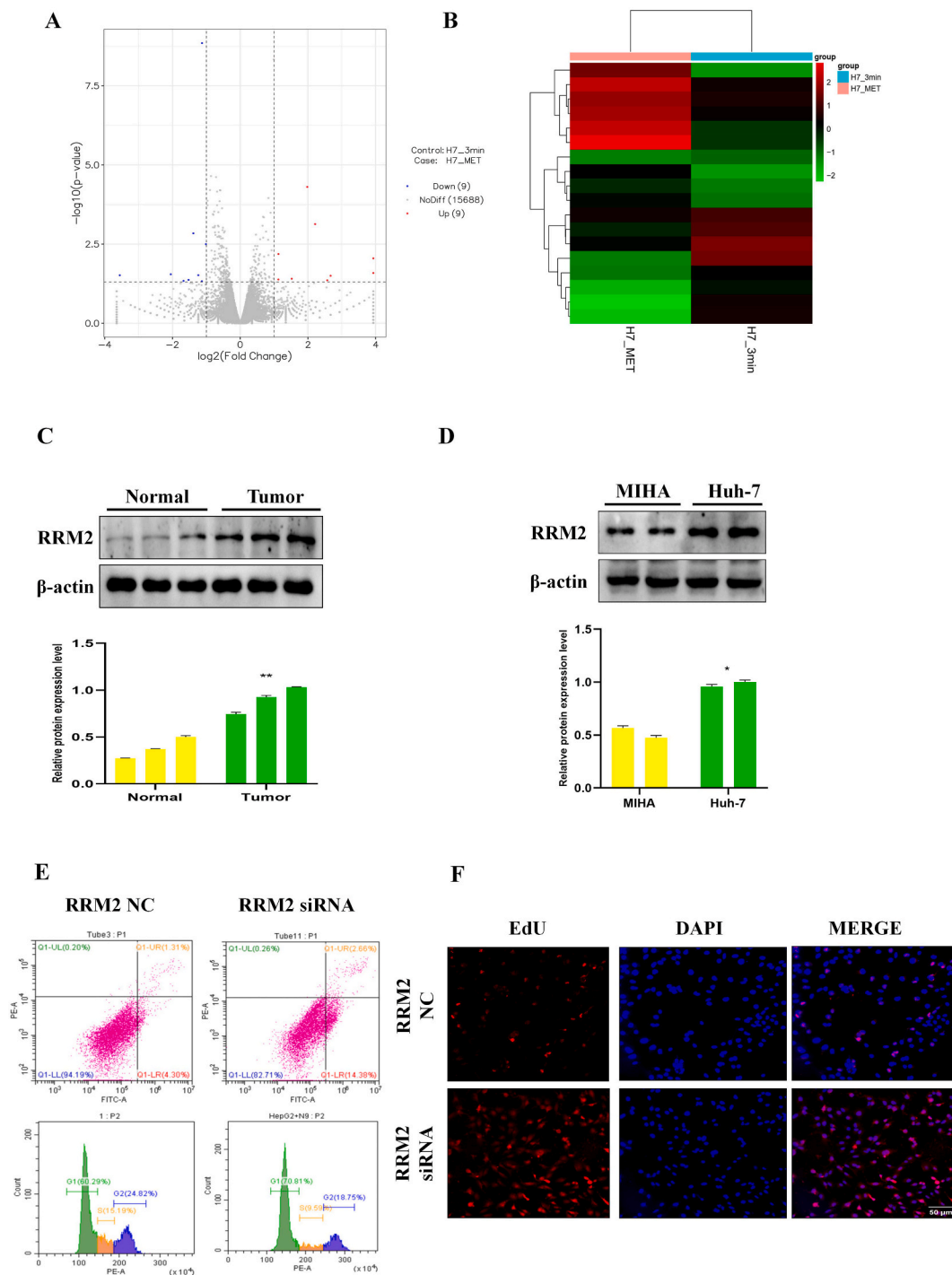


Fig. 3. (A) The volcano plot results show that 9 up-regulated genes and 9 down-regulated genes in H7_MET group compared with H7_3min group; (B) The results of heat map analysis showed differences in cellular gene expression under the influence of MEL and NTP-treated MEL; (C) RRM2 gene expression was upregulated in HCC tissues compared with adjacent liver tissues (Supplementary file 1); (D) RRM2 gene expression was upregulated in Huh-7 cells compared with MIHA cells (Supplementary file 1); (E) Flow cytometry found that the apoptosis rate of Huh-7 cells was significantly higher in the RRM2 siRNA group compared with RRM2 NC; (F) Edu staining showed that RRM2 siRNA inhibited the proliferation of Huh-7 cells.

redox signal changes in HCC cells. Our results showed that NTP-treated MEL was more effective at increasing ROS levels in HCC cells than MEL without NTP treatment. We speculate that this may be because NTP treatment alters the content of key oxidative functional groups in MEL. In the present study, we explored other molecular mechanisms underlying the synergistic effect of NTP and MEL on

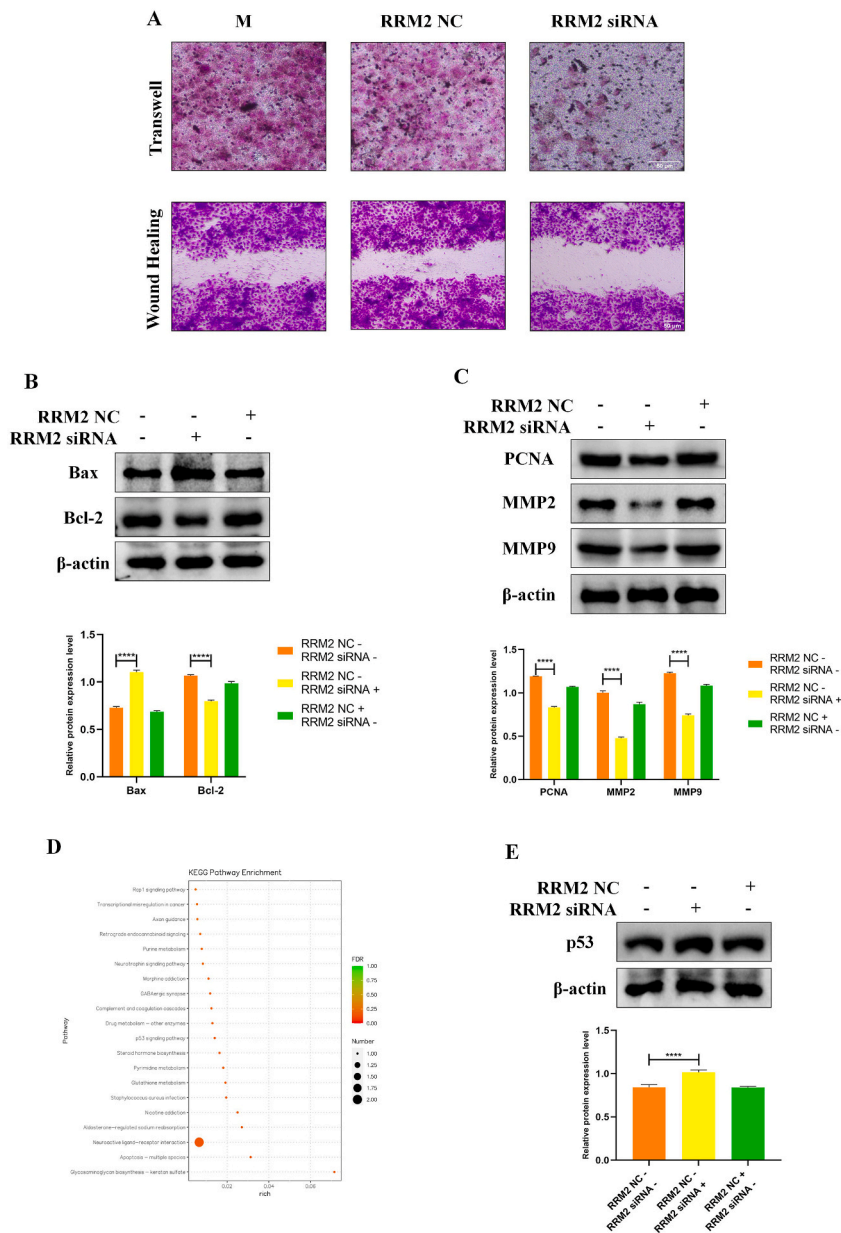


Fig. 4. (A) Transwell and wound healing assays showed that RRM2 siRNA significantly inhibited Huh-7 cell invasion and migration (The scratch area was 13774.483, 27297.46, 54691.403 μm^2 in turn from left to right); (B) Western blotting showed that RRM2 siRNA increased the expression of Bax and inhibited the expression of Bcl-2 in Huh-7 cells (Supplementary file 1); (C) Western blotting showed that RRM2 siRNA inhibited the expression of PCNA, MMP2 and MMP9 in Huh-7 cells (Supplementary file 1); (D) KEGG pathway enrichment analysis found that p53 may be a downstream signaling pathway of RRM2; (E) Western blotting showed that RRM2 siRNA increased the expression of p53 in Huh-7 cells, which confirmed that p53 is a downstream signaling pathway of RRM2 (Supplementary file 1).

HCC.

We used NTP to treat MEL for different durations to stimulate the HCC cell lines HepG2 and Huh-7. The results of the CCK8 assay showed that NTP treatment of MEL improved the effects of MEL on cell viability, but the duration of NTP treatment should be greater than 3 min. Additionally, flow cytometric analysis showed that the apoptosis rate of HCC cells stimulated with NTP-treated MEL increased significantly. EdU staining confirmed that NTP-treated MEL could better inhibit HCC cell proliferation, possibly by increasing the proportion of cells in the G1 phase. Wound healing and transwell assays confirmed that NTP-treated MEL had a better inhibitory effect on the invasion and migration of HCC cells than untreated MEL. To further explore the molecular mechanism, we screened DEGs during MEL and NTP-treated MEL treatments through transcriptome sequencing. We concluded that RRM2 may be an important site of action during the synergistic treatment with NTP and MEL. To explore and verify the role of RRM2, we performed

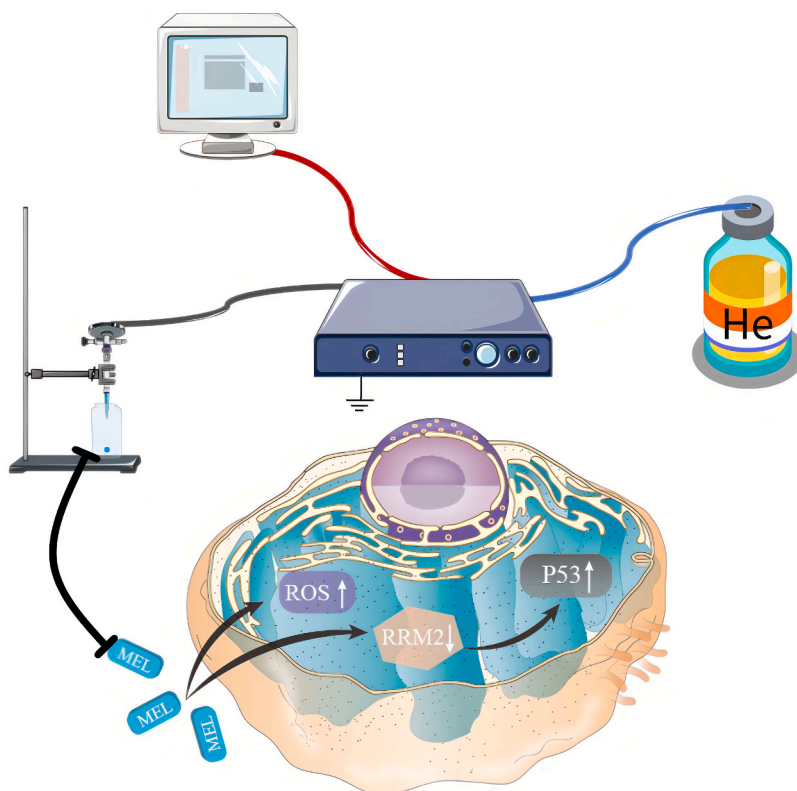


Fig. 5. NTP-treated MEL could regulate intracellular ROS levels and expression of RRM2 and p53, thereby promoting HCC cell apoptosis, delaying cell cycle progression, and inhibiting cell invasion and migration.

flow cytometry, EdU staining, JC-1 staining, Caspase 3 immunofluorescence staining, TUNEL staining, transwell assays, and wound healing assays. These results confirmed that RRM2 promotes the tumor characteristics of HCC cells. KEGG enrichment pathway analysis based on transcriptome sequencing predicted that the p53 pathway might be the downstream pathway of RRM2, which was confirmed by subsequent western blotting (Figure S2). Some studies have shown that NTP directly induces apoptosis in HCC cells by downregulating STAT1 and p53 [39].

Current drug treatments for cancer face many challenges that require careful consideration and improvement. One major issue is the toxicity of chemotherapeutic drugs, which can limit the effectiveness of treatment despite the various treatment options available [40,41]. Using nanotechnology to increase drug solubility may help overcome this challenge by opening new avenues for therapeutic development [42]. MEL in our study was found to be very safe, and NTP treatment can often improve drug solubility, providing a means for solving this problem.

Owing to the limited sample size, this study requires further verification. In future studies, we aim to explore additional mechanisms to build a more complete regulatory network. Further questions are also worth exploring, such as why NTP increases the *anti*-HCC efficacy of MEL. We will also verify the feasibility of this treatment combination for other tumor types. Tumor necrosis factor-related apoptosis-inducing ligand (TRAIL) selectively induces apoptosis in cancer cells and is currently regarded as a potential target for cancer therapy [43]. Whether a relationship exists between NTP, MEL, and TRAIL warrants investigation.

5. Conclusion

In conclusion, our study demonstrates the potential of NTP in combination with MEL as a promising therapeutic strategy for the treatment of HCC. NTP assists MEL in promoting apoptosis, delaying cell cycle progression, and inhibiting cell invasion and migration in HCC cells. Regulation of ROS levels and RRM2 expression may be involved in the mechanisms underlying these observed effects. Our study sheds new light on HCC treatment and highlights the need for further research to fully elucidate the potential of NTP and MEL in cancer therapy.

Author contribution statement

Bangjie Chen; Tao Jin: Performed the experiments; Wrote the paper.
Ziyue Fu; Haiwen Li: Analyzed and interpreted the data.

Junfa Yang, Yucheng Liu, Yanxun Han; Xinyi Wang: Performed the experiments.
Zhengwei Wu; Tao Xu: Conceived and designed the experiments; Contributed reagents, materials, analysis tools or data.

Data availability statement

No data was used for the research described in the article.

Declaration of competing interest

The authors declare that they have no known competing financial interests or personal relationships that could have appeared to influence the work reported in this paper.

Appendix A. Supplementary data

Supplementary data to this article can be found online at <https://doi.org/10.1016/j.heliyon.2023.e15992>.

References

- [1] M. Moreau, N. Orange, M.G. Feuilloley, Non-thermal plasma technologies: new tools for bio-decontamination, *Biotechnol. Adv.* 26 (2008) 610–617, <https://doi.org/10.1016/j.biotechadv.2008.08.001>, 2008/09/09.
- [2] J. De Backer, A. Lin, W.V. Berghe, et al., Cytochrome c inhibits non-thermal plasma-induced apoptosis in melanoma cells through regulation of the NRF2-mediated antioxidant response, *Redox Biol.* 55 (2022), 102399, <https://doi.org/10.1016/j.redox.2022.102399>, 2022/07/20.
- [3] S. Bekeschus, Combined toxicity of gas plasma treatment and nanoparticles exposure in melanoma cells in vitro, *Nanomaterials* 11 (2021), <https://doi.org/10.3390/nano11030806>, 2021/04/04.
- [4] M. Vandamme, E. Robert, S. Lerondel, et al., ROS implication in a new antitumor strategy based on non-thermal plasma, *Int. J. Cancer* 130 (2012) 2185–2194, <https://doi.org/10.1002/ijc.26252>, 2011/06/28.
- [5] S.Y. Kim, H.J. Kim, H.J. Kim, et al., Non-thermal plasma induces antileukemic effect through mTOR ubiquitination, *Cells* 9 (2020), <https://doi.org/10.3390/cells9030595>, 2020/03/07.
- [6] L. Shi, F. Ito, Y. Wang, et al., Non-thermal plasma induces a stress response in mesothelioma cells resulting in increased endocytosis, lysosome biogenesis and autophagy, *Free Radic. Biol. Med.* 108 (2017) 904–917, <https://doi.org/10.1016/j.freeradbiomed.2017.04.368>, 2017/05/04.
- [7] A. Forner, M. Reig, J. Bruix, Hepatocellular carcinoma, *Lancet* 391 (2018) 1301–1314, [https://doi.org/10.1016/S0140-6736\(18\)30010-2](https://doi.org/10.1016/S0140-6736(18)30010-2), 2018/01/09.
- [8] G.V. Papatheodoridis, V. Lekakis, T. Voulgaris, et al., Hepatitis B virus reactivation associated with new classes of immunosuppressants and immunomodulators: a systematic review, meta-analysis, and expert opinion, *J. Hepatol.* 77 (2022) 1670–1689, <https://doi.org/10.1016/j.jhep.2022.07.003>, 2022/07/20.
- [9] H. Sun, B. Yang, H. Zhang, et al., RRM2 is a potential prognostic biomarker with functional significance in glioma, *Int. J. Biol. Sci.* 15 (2019) 533–543, <https://doi.org/10.7150/ijbs.30114>, 2019/02/13.
- [10] W.X. Chen, L.G. Yang, L.Y. Xu, et al., Bioinformatics analysis revealing prognostic significance of RRM2 gene in breast cancer, *Biosci. Rep.* 39 (2019), <https://doi.org/10.1042/BSR20182062>, 2019/03/23.
- [11] Y.Z. Mazzu, J. Armenia, G. Chakraborty, et al., A novel mechanism driving poor-prognosis prostate cancer: overexpression of the DNA repair gene, ribonucleotide reductase small subunit M2 (RRM2), *Clin. Cancer Res.* 25 (2019) 4480–4492, <https://doi.org/10.1158/1078-0432.CCR-18-4046>, 2019/04/19.
- [12] Z. Zhou, Y. Li, H. Hao, et al., Screening hub genes as prognostic biomarkers of hepatocellular carcinoma by bioinformatics analysis, *Cell Transplant.* 28 (2019) 765–86S, <https://doi.org/10.1177/0963689719893950>, 2019/12/12.
- [13] W.H. Talib, Melatonin and cancer hallmarks, *Molecules* 23 (2018), <https://doi.org/10.3390/molecules23030518>, 2018/03/03.
- [14] D. Acuna-Castroviejo, G. Escames, C. Venegas, et al., Extrapineal melatonin: sources, regulation, and potential functions, *Cell. Mol. Life Sci.* 71 (2014) 2997–3025, <https://doi.org/10.1007/s00018-014-1579-2>, 2014/02/21.
- [15] R.M. Slominski, R.J. Reiter, N. Schlabritz-Loutsevitch, et al., Melatonin membrane receptors in peripheral tissues: distribution and functions, *Mol. Cell. Endocrinol.* 351 (2012) 152–166, <https://doi.org/10.1016/j.mce.2012.01.004>, 2012/01/17.
- [16] F. Luchetti, B. Canonico, M. Betti, et al., Melatonin signaling and cell protection function, *Faseb. J.* 24 (2010) 3603–3624, <https://doi.org/10.1096/fj.10-154450>, 2010/06/11.
- [17] A. Cutando, A. Lopez-Valverde, S. Arias-Santiago, et al., Role of melatonin in cancer treatment, *Anticancer Res.* 32 (2012) 2747–2753, 2012/07/04.
- [18] Y.Q. Gong, F.T. Hou, C.L. Xiang, et al., The mechanisms and roles of melatonin in gastrointestinal cancer, *Front. Oncol.* 12 (2022) 1066698, <https://doi.org/10.3389/fonc.2022.1066698>, 2023/01/03.
- [19] J. Florido, L. Martinez-Ruiz, C. Rodriguez-Santana, et al., Melatonin drives apoptosis in head and neck cancer by increasing mitochondrial ROS generated via reverse electron transport, *J. Pineal Res.* 73 (2022) e12824, <https://doi.org/10.1111/jpi.12824>, 2022/08/21.
- [20] A. Davoodvandi, B. Nikfar, R.J. Reiter, et al., Melatonin and cancer suppression: insights into its effects on DNA methylation, *Cell. Mol. Biol. Lett.* 27 (2022) 73, <https://doi.org/10.1186/s11658-022-00375-z>, 2022/09/06.
- [21] E.J. Sanchez-Barcelo, M.D. Mediavilla, C. Alonso-Gonzalez, et al., Melatonin uses in oncology: breast cancer prevention and reduction of the side effects of chemotherapy and radiation, *Expert Opin. Invest. Drugs* 21 (2012) 819–831, <https://doi.org/10.1517/13543784.2012.681045>, 2012/04/17.
- [22] I.D. Nagtegaal, R.D. Odze, D. Klimstra, et al., The 2019 WHO classification of tumours of the digestive system, *Histopathology* 76 (2020) 182–188, <https://doi.org/10.1111/his.13975>, 2019/08/23.
- [23] L. European Association For The Study Of The, R. European Organisation For, C. Treatment Of, EASL-EORTC clinical practice guidelines: management of hepatocellular carcinoma, *J. Hepatol.* 56 (2012) 908–943, <https://doi.org/10.1016/j.jhep.2011.12.001>, 2012/03/20.
- [24] S. Sangkaew, S. Wanmasae, K. Bunluepeuch, et al., Development of nanoemulsions for wound dressings containing Cassia alata L. Leaf extraction, *Evid Based Complement Alternat Med* 2022 (2022) 4282678, <https://doi.org/10.1155/2022/4282678>, 2022/10/22.
- [25] P. Pooprommin, C. Manaspon, A. Dwivedi, et al., Alginate/pectin dressing with niosomal mangosteen extract for enhanced wound healing: evaluating skin irritation by structure-activity relationship, *Heliyon* 8 (2022), e12032, <https://doi.org/10.1016/j.heliyon.2022.e12032>, 2022/12/13.
- [26] Z. Xin, S. Jiang, P. Jiang, et al., Melatonin as a treatment for gastrointestinal cancer: a review, *J. Pineal Res.* 58 (2015) 375–387, <https://doi.org/10.1111/jpi.12227>, 2015/03/11.
- [27] W. Li, M. Fan, Y. Chen, et al., Melatonin induces cell apoptosis in AGS cells through the activation of JNK and P38 MAPK and the suppression of nuclear factor-kappa B: a novel therapeutic implication for gastric cancer, *Cell. Physiol. Biochem.* 37 (2015) 2323–2338, <https://doi.org/10.1159/000438587>, 2015/12/10.
- [28] V. Srinivasan, D.W. Spence, S.R. Pandi-Perumal, et al., Therapeutic actions of melatonin in cancer: possible mechanisms, *Integr. Cancer Ther.* 7 (2008) 189–203, <https://doi.org/10.1177/1534735408322846>, 2008/09/26.

- [29] Y. Li, S. Li, Y. Zhou, et al., Melatonin for the prevention and treatment of cancer, *Oncotarget* 8 (2017) 39896–39921, <https://doi.org/10.18632/oncotarget.16379>, 2017/04/19.
- [30] S.M. Hill, V.P. Belancio, R.T. Dauchy, et al., Melatonin: an inhibitor of breast cancer, *Endocr. Relat. Cancer* 22 (2015) R183–R204, <https://doi.org/10.1530/ERC-15-0030>, 2015/04/17.
- [31] A. Carrillo-Vico, J.M. Guerrero, P.J. Lardone, et al., A review of the multiple actions of melatonin on the immune system, *Endocrine* 27 (2005) 189–200, <https://doi.org/10.1385/ENDO:27:2:189>, 2005/10/12.
- [32] R.J. Reiter, S.A. Rosales-Corral, D.X. Tan, et al., Melatonin, a full service anti-cancer agent: inhibition of initiation, progression and metastasis, *Int. J. Mol. Sci.* 18 (2017), <https://doi.org/10.3390/ijms18040843>, 2017/04/20.
- [33] H. Kajiyama, F. Utsumi, K. Nakamura, et al., Future perspective of strategic non-thermal plasma therapy for cancer treatment, *J. Clin. Biochem. Nutr.* 60 (2017) 33–38, <https://doi.org/10.3164/jcbn.16-65>, 2017/02/07.
- [34] H. Tanaka, M. Mizuno, K. Ishikawa, et al., Molecular mechanisms of non-thermal plasma-induced effects in cancer cells, *Biol. Chem.* 400 (2018) 87–91, <https://doi.org/10.1515/hsz-2018-0199>, 2018/10/07.
- [35] E.H. Sarsour, M.G. Kumar, L. Chaudhuri, et al., Redox control of the cell cycle in health and disease, *Antioxidants Redox Signal.* 11 (2009) 2985–3011, <https://doi.org/10.1089/ARS.2009.2513>, 2009/06/10.
- [36] S. Toyokuni, K. Okamoto, J. Yodoi, et al., Persistent oxidative stress in cancer, *FEBS Lett.* 358 (1995) 1–3, [https://doi.org/10.1016/0014-5793\(94\)01368-b](https://doi.org/10.1016/0014-5793(94)01368-b), 1995/01/16.
- [37] S. Toyokuni, The origin and future of oxidative stress pathology: from the recognition of carcinogenesis as an iron addiction with ferroptosis-resistance to non-thermal plasma therapy, *Pathol. Int.* 66 (2016) 245–259, <https://doi.org/10.1111/pin.12396>, 2016/03/05.
- [38] W.P. Roos, B. Kaina, DNA damage-induced cell death: from specific DNA lesions to the DNA damage response and apoptosis, *Cancer Lett.* 332 (2013) 237–248, <https://doi.org/10.1016/j.canlet.2012.01.007>, 2012/01/21.
- [39] B. Smolkova, M. Lunova, A. Lynnyk, et al., Non-thermal plasma, as a new physicochemical source, to induce redox imbalance and subsequent cell death in liver cancer cell lines, *Cell. Physiol. Biochem.* 52 (2019) 119–140, <https://doi.org/10.33594/000000009>, 2019/02/23.
- [40] K. Sak, Chemotherapy and dietary phytochemical agents, *Chemother Res Pract* 2012 (2012), 282570, <https://doi.org/10.1155/2012/282570>, 2013/01/16.
- [41] J.S. Arya, M.M. Joseph, D.R. Sherin, et al., Exploring mitochondria-mediated intrinsic apoptosis by new phytochemical entities: an explicit observation of cytochrome c dynamics on lung and melanoma cancer cells, *J. Med. Chem.* 62 (2019) 8311–8329, <https://doi.org/10.1021/acs.jmedchem.9b01098>, 2019/08/09.
- [42] M.M. Joseph, S.R. Aravind, S.K. George, et al., Anticancer activity of galactoxyloglucan polysaccharide-conjugated doxorubicin nanoparticles: mechanistic insights and interactome analysis, *Eur. J. Pharm. Biopharm.* 93 (2015) 183–195, <https://doi.org/10.1016/j.ejpb.2015.04.001>, 2015/04/14.
- [43] S.R. Aravind, M.M. Joseph, S.K. George, et al., TRAIL-based tumor sensitizing galactoxyloglucan, a novel entity for targeting apoptotic machinery, *Int. J. Biochem. Cell Biol.* 59 (2015) 153–166, <https://doi.org/10.1016/j.biocel.2014.11.019>, 2014/12/30.